ADVANCED BIOLOGY
www.advanced-bio.com

Modeling Foam Cell Formation in A Hydrogel-Based 3D-Intimal Model: A Study of The Role of Multi-Diseases During Early Atherosclerosis

*Fahima Akther, Dimple Sajin, Shehzahdi S. Moonshi, Yuao Wu, Karla X Vazquez-Prada, and Hang Thu Ta**

Monocyte recruitment and transmigration are crucial in atherosclerotic plaque development. The multi-disease complexities aggravate the situation and continue to be a constant concern for understanding atherosclerosis plaque development. Herein, a 3D hydrogel-based model that integrates disease-induced microenvironments is sought to be designed, allowing us to explore the early stages of atherosclerosis, specifically examining monocyte fate in multi-disease complexities. As a proof-of-concept study, murine cells are employed to develop the model. The model is constructed with collagen embedded with murine aortic smooth muscle cells and a murine endothelial monolayer lining. The model achieves in vitro disease complexities using external stimuli such as glucose and lipopolysaccharide (LPS). Hyperglycemia exhibits a significant increase in monocyte adhesion but no enhancement in monocyte transmigration and foam cell conversion compared to euglycemia. Chronic infection achieved by LPS stimulation results in a remarkable augment in initial monocyte attachment and a significant increment in monocyte transmigration and foam cells in all concentrations. Moreover, the model exhibits synergistic sensitivity under multi-disease conditions such as hyperglycemia and infection, enhancing initial monocyte attachment, cell transmigration, and foam cell formation. Additionally, western blot data prove the enhanced levels of inflammatory biomarkers, indicating the model's capability to mimic disease-induced complexities during early atherosclerosis progression.

1. Introduction

Atherosclerosis is a multistage, slowly progressive disorder associated with self-amplifying cell-cell interaction.[1] A pivotal event in atherogenesis occurs when monocytes adhere to the endothelium and transmigrate into the subendothelial space, differentiating into macrophages.[2–6] A subsequent conversion of macrophages to foam cells occurs after oxidized (ox)- lipid accumulation in the intimal layer. These lipid-laden foam cells play a critical pathogenic role in atherosclerotic plaque development.[7–12] The multifactorial complexities linked with atherosclerosis draw attention to the investigators to understand the mechanism behind how monocytes reach the arterial wall, transmigrate across the endothelium, form foam cells inside the intima, and remove lipids to trigger atherosclerosis plaque development.[13] Evidence strongly suggests factors like hyperglycemia and chronic infection have been postulated to cause microvascular and macrovascular complications, including atherosclerosis.[14,15]

F. Akther, D. Sajin, S. S. Moonshi, Y. Wu, K. X Vazquez-Prada, H. T. Ta
Queensland Micro- and Nanotechnology
Griffith University
Nathan, Queensland 4111, Australia
E-mail: h.ta@griffith.edu.au

F. Akther, K. X Vazquez-Prada, H. T. Ta
Australian Institute for Bioengineering and Nanotechnology
The University of Queensland
St Lucia, Queensland 4072, Australia

H. T. Ta
School of Environment and Science
Griffith University
Nathan, Queensland 4111, Australia

The ORCID identification number(s) for the author(s) of this article can be found under https://doi.org/10.1002/adbi.202300463

DOI: 10.1002/adbi.202300463

Atherosclerosis development is accelerated by two to four-fold compared to those without diabetes.[16,17] Hyperglycemia could cause cellular alteration, including non-enzymatic glycosylation of proteins and lipids, oxidative stress, and activation of protein kinase C (PKC), which could alter growth factor expression.[18] Increased expression of vascular cell adhesion molecules in the diabetic endothelial cell has been shown in in vitro[19] and in vivo studies.[20] Short-term hyperglycemia promotes monocyte adhesion to rat thoracic aorta[21] and human aortic endothelial cells.[14] Moreover, infection is found to be a risk factor for atherosclerosis and contributes to chronic inflammatory processes either directly or indirectly.[22] A direct effect would be demonstrated by the ability of the organisms to infect vascular cells, by their presence within atherosclerotic plaques, and by a rapid progression of lesions following infection in animal models of atherosclerosis. On the other hand, infections at non-vascular sites could indirectly affect atherosclerosis through the release of cytokines and other acute-phase proteins.[22,23] The presence of chronic infections can be a contributing factor to approximately 40% of new-onset atherosclerosis.[24] It has been suggested that lipopolysaccharide (LPS), an endotoxin produced by bacteria, is responsible for atherogenesis by activating inflammatory cells.[25,26]

There is a constant need to develop physiologically relevant in vitro biomimetic models for studying multistep atherogenesis processes in patient-specific conditions. The commonly used in vitro model for studying monocyte transmigration is two-dimensional (2D) trans well systems composed of polycarbonate membrane with pore sizes ranging from 3–8 μm.[3,14,27–31] Trans well models use chemotaxis to initiate monocyte transmigration and oxidized low-density protein (ox-LDL) to induce lipid-laden foam cells.[2,32] Although such systems possess some benefits, their use is limited due to the absence of a physiological microenvironment. A recent advancement to eliminate the gaps is the three-dimensional (3D) hydrogel-based in vitro models. Such models can mimic the cell-cell and cell-matrix environment that ratify precision in mimicking the atherogenic microenvironment. William Muller[33] first reported a 3D collagen-based coculture model with a collagen construct and a lining of human umbilical vein endothelial cells (HUVEC) on the collagen construct for studying monocyte transendothelial migration in 1992. The model allowed the selective transmigration of monocytes by crossing the endothelial monolayer within the collagen construct without any external chemoattractant or endothelial activation. The same model was employed by Nandy et al.[34] to investigate the effects of hyperglycemia on the activation of human monocytes. The study found that hyperglycemia substantially enhanced monocyte adhesion to endothelium and transendothelial migration by increasing pseudopodia formation. Moreover, the study suggested that hyperglycemia upregulated the phosphorylation of p101 and p110γ subunits of PI-3 kinase in monocytes. Inhibition of PI-3 kinase could reduce the hyperglycaemic-induced monocyte transmigration. Angelovich et al.[35] used the similar hydrogel-based coculture model to investigate the effect of age in monocyte modification for foam cell formation and later extended the use to quantify the monocyte transmigration and foam cell formation with chronic inflammatory conditions.[36] The potential role of HIV-derived high-density lipoprotein (HDL) in monocyte-derived foam cell formation was also investigated in such a model.[37]

A fibrillar collagen-based model with embedded THP-1 cell line, aimed to replicate the low and high tissue density to investigate the effects of extracellular matrix (ECM) proteins in LDL uptake, phenotypic gene expression, and adipokines secretion.[38] Moreover, most previous studies overlooked the importance of rational growth of vascular smooth muscle cells in the atherosclerosis intima. A recent study (published in January 2023), however, considered the role of vascular smooth muscle cells (VSMCs) in atherosclerosis by developing a collagen-based coculture model with vascular and inflammatory cells to study the effects of shear stress on native LDL oxidation and pro-inflammatory molecules released during atherosclerosis.[39] The model embedded VSMCs in the collagen construct to represent pathological intimal thickening. However, the major limitation of this model is that the total preparation time of this coculture system is only 24 h. The study seeded the HUVEC on the top of the collagen construct for 2 h and then immediately added native LDL and THP-1 monocytes to observe LDL diffusion and monocyte migration. It is not feasible that the EC intact integrity was achieved in 2 h. The cells might attach in 2 h, but it requires time to proliferate and develop tight cell junctions. Studies suggested approximately 5–7 days of incubation to get the endothelial integrity on the hydrogel construct.[35–37] Since they added monocytes to the coculture system before confirming the tight endothelial junction, there was a high chance that the monocytes diffused into the hydrogel layer instead of subendothelial transmigration. Also, the model wanted to achieve the intimal thickening only by adding VSMCs in the collagen. Atherosclerosis intima thickening requires VSMCs proliferation and matrix protein deposition in the intima,[40] which was not possible by 24 h incubation time[41] and was overlooked by this model.

The current study gaps suggested developing an atherosclerosis-inspired intimal model considering the coculture longevity and vascular cell involvement. Alongside, it is essential to note that pathological conditions, such as diabetes, dyslipidemia, hypertension, and infections, directly or indirectly affect the inflammatory cell kinetics, LDL permeability, and oxidation,[38] thus modulating atherosclerosis plaque formation. The development of patient-specific 3D-atherosclerosis models that incorporate the individual's risk and potency in foam cell formation or plaque formation has yet to be studied. Considering the existing gaps, we sought to develop a 3D hydrogel-based coculture model where collagen was embedded with vascular smooth muscle cells and coated with an endothelial monolayer, mimicking the intimal layer (**Figure 1**). The coculture model allows the long-time incubation to replicate the atherosclerosis intimal thickening with endothelial junction integrity. This simple but robust model provides a unique platform to replicate the disease-induced conditions to study the ultimate fate of monocytes in atherosclerosis plaque development. The immune-vascular interplay in this model replicates the individual risk in monocyte adhesion and transendothelial migration. Additionally, subendothelial lipid accumulation is achieved by adding native LDL instead of ox-LDL in the culture media, which proves advantageous to mimic more accurate physiology in 3D in vitro conditions. Similar to the in vivo system, LDL oxidation

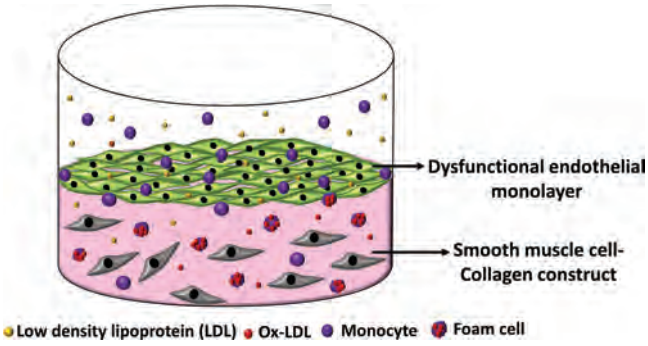

Figure 1. Schematic presentation of the 3D-atherosclerosis intimal model. The collagen hydrogel-smooth muscle cell construct lining with endothelial monolayers replicates the early atherosclerosis intima. Dysfunctional endothelium triggers initial monocyte adhesion and transmigration into subendothelial intima. The transmigrated cells uptake oxidized LDL to convert into lipid-laden foam cells.

can happen in subendothelial space in the coculture system, and a significant number of foam cells are detected in single and multiple disease conditions. The secretion of inflammatory biomarkers associated with atherosclerosis pathogenicity in single and multi-disease conditions also proves the model's validity. In the future, the model might be useful to evaluate the patient-specific risk in atherosclerosis pathogenesis.

2. Results

2.1. Cell Viability/Metabolic Activity in Different Treatment Conditions and Time Points

Cell viability/metabolic activity of all 3 cell lines was checked in different treatment conditions and at different time points to determine the appropriate experimental conditions. All cell lines were healthy and maintained above 80% viable up to 8 h of treatment in all treated groups (**Figure 2**). However, MOVAS and RAW 264.7 cell lines showed a slight reduction in the LPS-treated group at 200 pg mL^{-1} (Figure 2D,F) at 12 h and recovered the viability and metabolic activity at 24 h incubation. RAW 264.7 cell lines also showed reduced viability in the LDL-treated group at 50 µg mL^{-1} at 12 h (Figure 2I). Overall, the viability/metabolic activity reduction was not dose-dependent and fluctuated at different concentrations and time points. Based on the data, we considered 8 h to be the optimal time for all remaining experiments.

2.2. Evaluation of Endothelial Integrity by Immunostaining

The SVEC-10 cells attached within an hour on the top of the MOVAS-collagen construct and showed elongated morphology. The cells grew over time and formed a confluent monolayer after six days of incubation. The cells exhibited a polygonal, compact morphology upon confluency on the MOVAS-collagen construct (**Figure 3A**).

An adherent junction of the confluent SVEC-10 monolayer was observed under a confocal microscope by immunostaining. The images suggested the associated risk in single and multi-disease conditions to initiate endothelial dysfunction. Four major groups: control (5.5 mM glucose without any additional treatment), severe hyperglycemia (25 mM D-glucose), chronic infection (200 pg mL^{-1} LPS), and the combination of hyperglycemia and infection (25 mM D-glucose + 50 pg mL^{-1} LPS) were used to check the junction leakiness upon treatment. An intact VE-cadherin junction of SVEC-10 was detected on the MOVAS-collagen construct in the control group (Figure 3B), proving the endothelium integrity in our intimal model. However, immunostaining confirmed some leakiness in the adherent junction of the SVEC-10 layer in the glucose-treated group (Figure 3C). Interestingly, a remarkable deterioration in the SVEC-10 monolayer and junction leakiness in several spots were detected in the LPS-treated group and marked by white arrows in Figure 3D, proving the endothelial dysfunction upon LPS treatment. The combination treatment with glucose and LPS also showed endothelial leakiness in various spots (Figure 3E), which was much more prominent than only the glucose group.

The TRITC-dextran cell-permeability assay was performed to further quantify the effective barrier integrity of endothelial monolayers upon treatment. The compromised integrity of the endothelial junctions facilitates the increased diffusion of TRITC-dextran macromolecules through the SVEC-10 monolayer into the MOVAS-collagen constructs, and this enhanced endothelium permeability can be measured by assessing the fluorescence intensity. The quantitative results of this assay, which included four major groups: the control group (5.5 mM glucose without any additional treatment), the severe hyperglycemia group (25 mM D-glucose), the chronic infection group (200 pg mL^{-1} LPS), and the group subjected to both hyperglycemia and infection (25 mM D-glucose + 50 pg mL^{-1} LPS), strongly confirmed the presence of increased leakage at the endothelial junctions observed in the microscopic images. A significant rise in fluorescence intensity was observed in all three treated groups in comparison to the control group (Figure 3F), providing clear evidence of compromised integrity in the endothelial junctions when exposed to both glucose and LPS.

2.3. Effects of Vascular Smooth Muscle Cells in Monocyte Transmigration and Foam Cell Conversion

This section focused on studying the effects of MOVAS in monocyte transmigration and potential responses in foam cell formation. The addition of MOVAS in the collagen construct to mimic the intimal layer enhanced the initial attachment of monocytes compared to the construct without MOVAS but the enhancement was not statistically significant (**Figure 4A**). Quantification of surface-bound monocytes/foam cells in both groups showed no remarkable differences (Figure 4B). However, a significant increase ($p<0.01$) in the percentage of transmigrated foam cells was recorded in the group with MOVAS. MOVAS-collagen constructs showed 10% more transmigrated foam cells than those without MOVAS (Figure 4C), while no comparable differences were noticed in the percentage of transmigrated non-foamy monocytes in both groups (Figure 4D). Foam cells and monocytes differed morphologically based on lipid accumulation. A distinct foamy morphology was detected upon lipid accumulation in the cell cytoplasm. Microscopic images confirmed foamy morphology in fixed cells in thin smears (Figure 4E) and

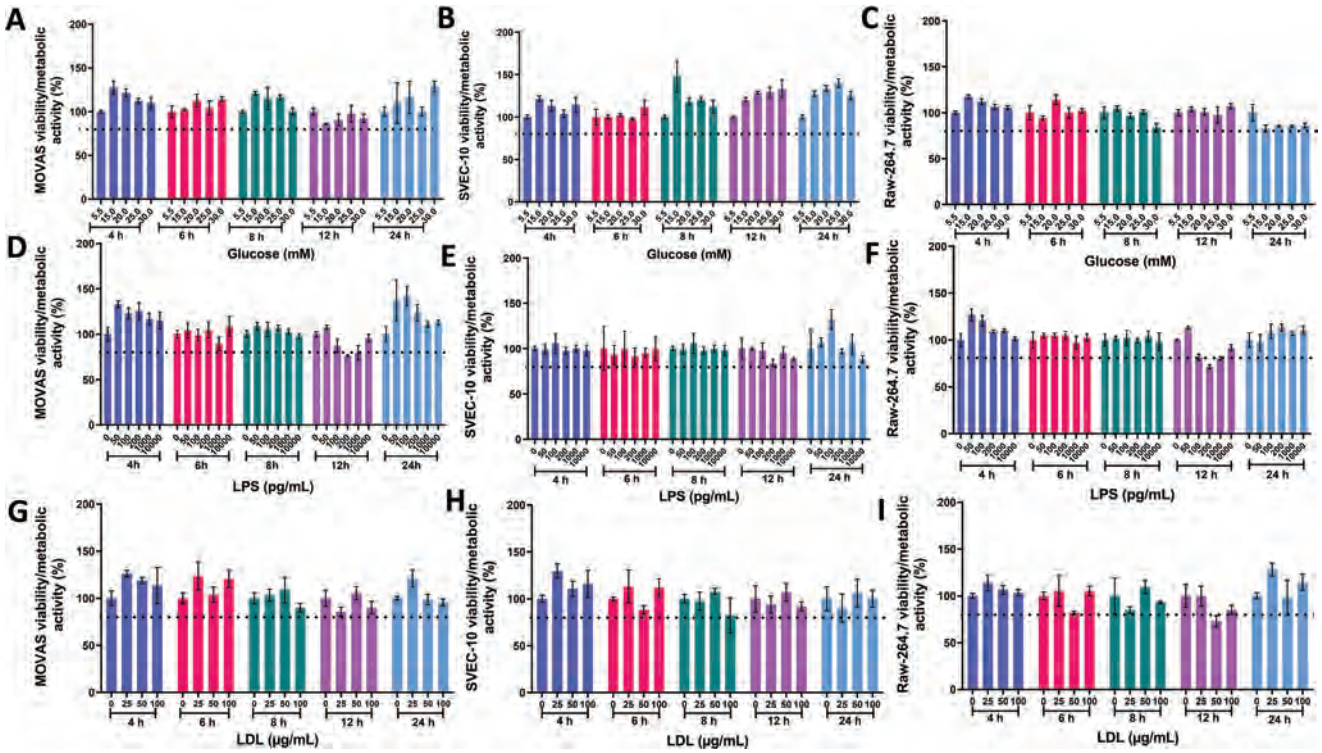

Figure 2. Cell viability/metabolic activity profiles under various treatment conditions and time points. The viability/metabolic activity of A) MOVAS, B) SVEC-10, and C) RAW 264.7 at various glucose concentrations and treatment times. Cell viability/metabolic activity profile of different cell lines such as D) MOVAS, E) SVEC-10, and F) RAW 264.7 in the LPS-treated groups at various time points. The viability/metabolic activity of G) MOVAS, H) SVEC-10, and I) RAW 264.7 in different LDL concentrations and treatment times.

fixed cells separated from the hydrogel construct in the solution (Figure 4F) due to lipid deposition (red/orange droplets) in the cell cytoplasm. In contrast, monocytes have rounded and smooth morphology without any lipid droplets. Monocytes/foam cells mainly showed rounded and oval morphology on the SVEC-10 monolayer on the collagen construct both with/without MOVAS (Figure 4G,I). However, the transmigrated cells exhibited spindle or rounded widespread morphology inside the collagen construct in both groups (Figure 4H,J).

An interesting finding was also observed. We counted the number of monocytes/foam cells transmigrated throughout the collagen construct and attached to the bottom of 96-well plates. The height of the collagen construct was ~1 mm. A significant increase in monocytes/foam cells number at the bottom of the well was noticed in the MOVAS-collagen construct group (Figure 4K) than in the construct without MOVAS. The presence of MOVAS might enhance the total migration distance or induce proliferation in transmigrated cells (Figure 4L,M).

2.4. Transmigration Study and Foam Cell Observation in Hyperglycaemic Condition

Quantitative data analysis revealed a significant increase in monocyte adhesion on the monolayer of SVEC-10 in hyperglycemia (15, 20, and 25 mM) in comparison to euglycemia (5.5 mM) (**Figure** 5A) after 1 h incubation. The 3D-coculture model was incubated for 48 h to initiate monocyte transmigration and foam cell formation. Representative graphs revealed no significant changes in the percentage of non-transmigrated monocytes/foam cells on the surface of cell construct (Figure 5B), transmigrated foam cells (Figure 5C), and transmigrated non-foamy monocytes (Figure 5D) in any of the treated groups after 48 h of incubation. The surface adherent monocytes/foam cells showed rounded and oval morphology, and the transmigrated cells showed elongated, polygonal, and widespread rounded morphology in all groups (Figure 5E–H). The images also confirmed no significant rise in surface adherent and transmigrated cell number in different glucose concentrations.

2.5. Transmigration Study and Foam Cell Observation in Infectious Condition

The quantitative data graph revealed a significant increase ($p<0.001$) in monocyte adhesion to SVEC-10 monolayer with LPS treatment at all concentrations after 1 h incubation (**Figure** 6A). Moreover, a remarkable reduction in the percentage of surface-bound monocytes/foam cells on the cell construct in the LPS-treated groups was detected after 48 h incubation (Figure 6B), indicating the increased transmigration of cells into the subendothelial intimal layer. The percentage of transmigrated foam cells increased in a dose-dependent manner (Figure 6C), whereas no distinguishable changes were observed in the percentage of the transmigrated non-foamy monocytes (Figure 6D) after 48 h. The microscopic images revealed the cell morphology and

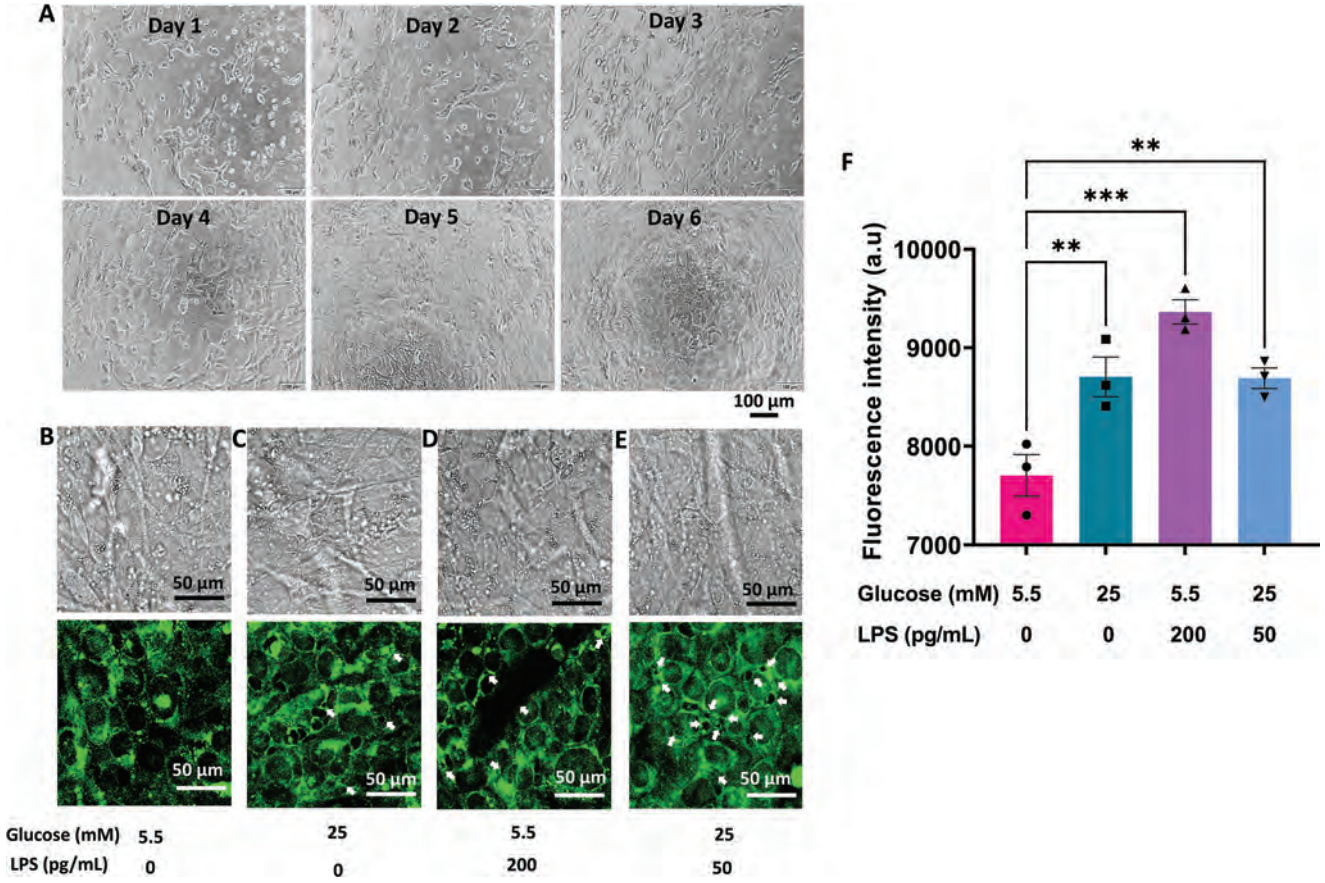

Figure 3. Formation of endothelial layer and evaluation of endothelial integrity. A) Growing of SVEC-10 cells and monolayer formation on the MOVAS-collagen construct. The cell grew and spread overtime on the 3D-MOVAS-collagen surface and formed a confluent monolayer after six days of incubation. Scale bar = 100 µm. (B-E) Endothelial junction integrity on the MOVAS-collagen constructs in different disease conditions. Alexa FluorTM 488 conjugated anti-Mo CD144 (VE-cadherin) monoclonal antibody (green) was used to detect the adherent junction of the SVEC-10 monolayer on MOVAS-collagen. B) The adherent monolayer of SVEC-10 on MOVAS-collagen construct in the control group. An intact endothelial network without any leakiness between cellular junctions was observed. C) The lining of SVEC-10 on MOVAS-collagen construct in severe hyperglycemia (25 mM). Random leakiness in the cell junction was noticed and marked by white arrows. D) Adherent monolayers of SVEC-10 in chronic infection (200 pg mL^{-1}). A visible deterioration in the SVEC-10 monolayer with junction leakiness was observed and marked by white arrows. E) The SVEC-10 monolayer on the MOVAS-collagen constructs in multi-disease conditions (25 mM Glucose + 50 pg mL^{-1} LPS). The junction leakiness was observed all over the SVEC-10 monolayer and marked by white arrows. F) TRITC-dextran cell-permeability assay to confirm endothelial integrity on MOVAS-collagen construct. TRITC-dextran diffusion into the MOVAS-collagen constructs was determined by measuring the fluorescence intensity at 555 nm. The fluorescence intensity significantly intensified in both glucose (25 mM glucose+ 0 pg mL^{-1} LPS), LPS (5.5 mM glucose+ 200 pg mL^{-1} LPS), and dual treated groups (25 mM glucose+ 50 pg mL^{-1} LPS) than that of control (5.5 mM glucose+ 0 pg mL^{-1} LPS). Values are mean ± SD, $n = 3$, one-way ANOVA. $^{**}p < 0.01$, and $^{***}p < 0.001$compared to the control.

showed a similar morphology to that of glucose-treated groups for both surface-bound and transmigrated cells. Surface-bound monocytes/foam cells showed a dose-dependent reduction, while transmigrated cells grew in number (Figure 6E–H).

2.6. Monocyte Transmigration and Foam Cell Formation in Multi-Disease Conditions

Glucose and LPS were added to the coculture model before monocyte addition to create multi-disease complexities, such as hyperglycemia and infection. The data graph showed an increase in adherent monocytes after 1 h incubation in all treatment conditions (**Figure** 7A). Significant depletion of surface adherent monocytes/foam cells was observed in 20 mM and 25 mM glucose+ LPS-treated groups, while no remarkable change was observed in the 15 mM glucose+ LPS-treated group after 48 h (Figure 7B). All treated groups showed a substantial increase in foam cell formation than the control. A significance of $p<0.0001$ was observed in the percentage of transmigrated foam cells in the 20 mM glucose+ LPS treated group, while a slight reduction was observed in the highest treated group (Figure 7C). The increased percentage of foam cell formation in the treated groups also confirmed the risk of atherosclerosis under infection conditions. Almost a 20% increase in the foam cell percentage was observed in the higher treatment concentrations (20 and 25 mM glucose with LPS) than that of 15 mM glucose+ LPS. It was also observed in all treated groups that non-foamy monocytes were significantly reduced compared to the control (Figure 7D). The surface-bound and the transmigrated cells showed a similar morphology as

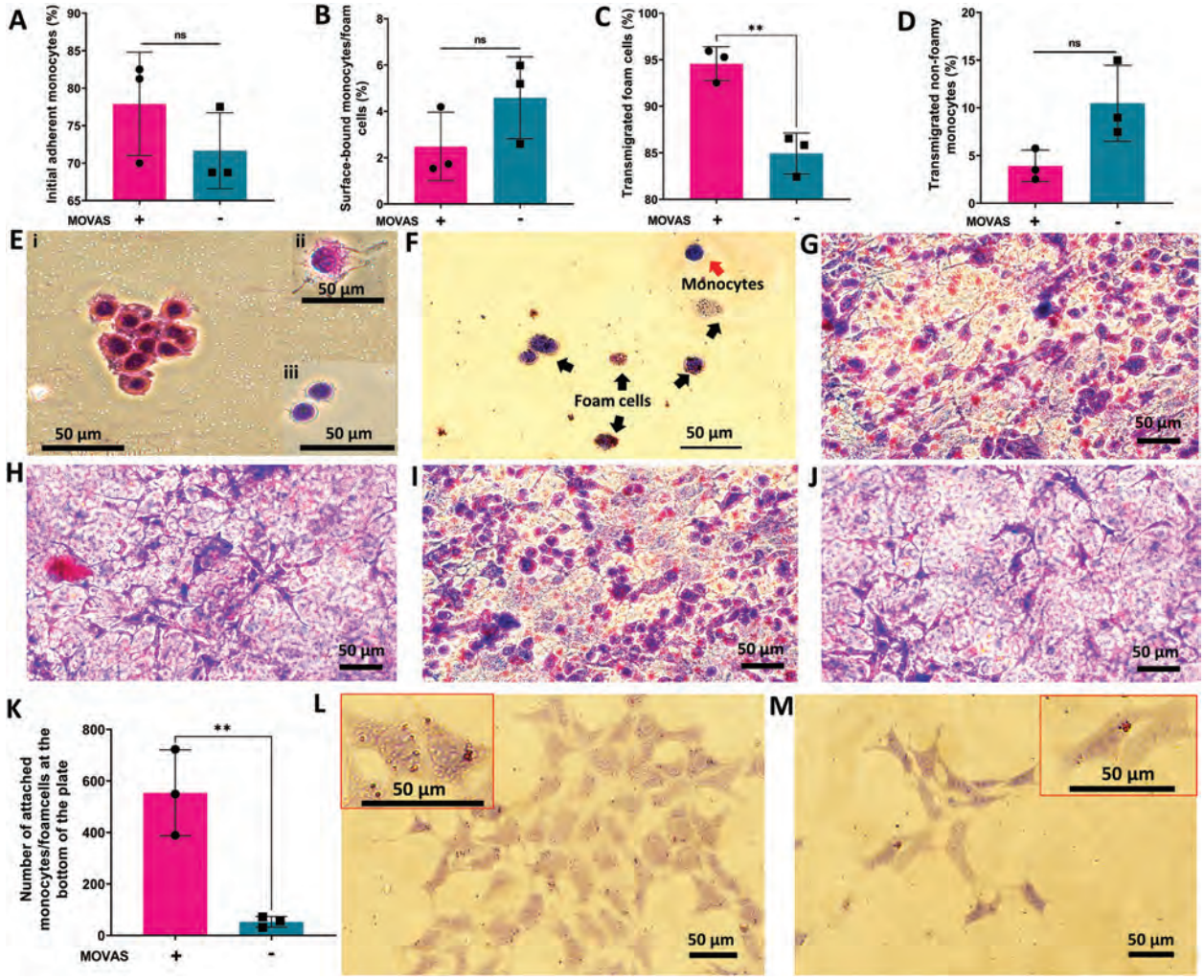

Figure 4. Effect of smooth muscle cells in monocyte transmigration and foam cell formation. A) Initial monocyte adhesion on the construct with/without MOVAS after 1 h of incubation. B) Percentage of surface monocytes/foam cells in total monocytes/foam cells count in the construct after 48 h incubation. No comparable difference was observed between groups. C) Transmigrated foam cell percentage in the cell construct. A significant rise in foam cell count was recorded in the cell construct with MOVAS. D) Percentage of non-foamy monocytes in the cell construct with/without MOVAS. Quantitative analysis showed no statistical difference. Values are mean ± SD, $n = 3$, t-test. $^{**}p < 0.01$, ns-not significant. E) Microscopic images of fixed foam cells (i, ii) and monocytes (iii) in the thin smear. A foamy morphology was detected due to the lipid deposition in the cell cytoplasm, while a smooth rounded morphology was observed for the monocytes. F) Image of fixed foam cells and monocytes in the solution. The lipid droplets were clearly visible in red in the foam cell and provided a granules-like morphology (Black arrow). The monocytes gave a strong purple color with apparently smooth rounded morphology (Red arrow). G) Monocytes/foam cells on the surface of the MOVAS-collagen construct after 48 h of incubation. The cells exhibited mostly rounded and oval morphology. H) Transmigrated monocytes/foam cells in MOVAS-collagen construct. The cells showed spindle and rounded widespread morphology. I) Monocytes/foam cells on the surface of the collagen construct without MOVAS after 48 h of incubation. J) Transmigrated monocytes/foam cells in collagen construct without MOVAS. The cell morphology was similar to that in the MOVAS-collagen construct group. KM) The number of adherent monocytes/foam cells at the bottom of the culture plate that transmigrated throughout the collagen construct. K) Quantitative analysis of the monocytes/foam cells number attached at the bottom of the plate. The cells would transmigrate throughout the collagen construct and attach to the bottom of the plate. A significant increase in the number of attached monocytes was found in the group with MOVAS compared to the group without MOVAS. Values are mean ± SD, $n = 3$, t-test, $^{**}p < 0.01$. Microscopic images of the attached monocytes/foam cells at the bottom of the wells in the group with MOVAS L) and without MOVAS M). An evident variation in the cell number was observed between the two groups. Lipid accumulation (red dot) was clearly visible under the microscope and confirmed the foam cell conversion.

those in the only glucose-treated groups. A dose-dependent reduction in surface-bound monocytes/foam cells and the increase in the transmigrated cells were confirmed by the microscopic images (Figure 7E–H).

2.7. Western Blot for Analyzing Protein Expression Profile

The expression of inflammatory proteins in the 3D-atherosclerosis intimal model, including IL- 1β, IL-6, TNF-α,

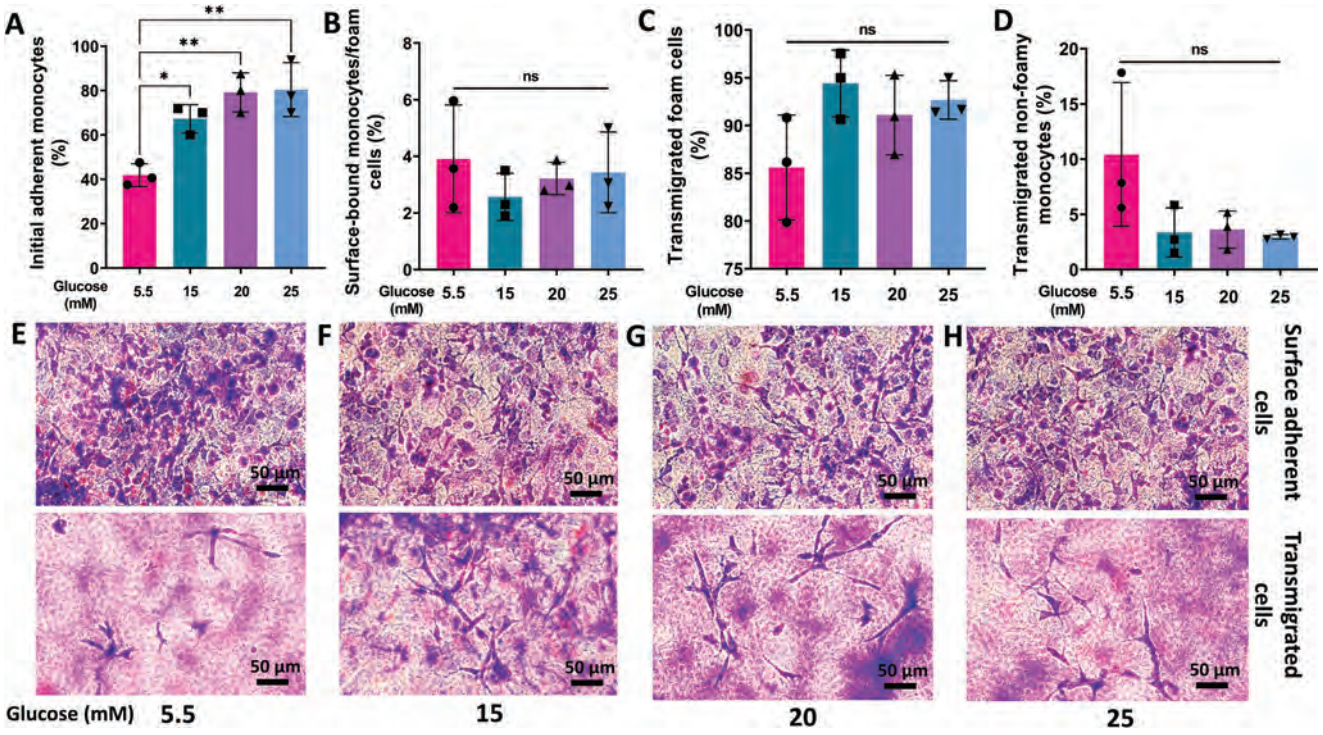

Figure 5. Effects of glucose on monocyte transmigration and foam cell formation in 3D- intimal model. A) Quantification of initial monocyte adhesion on the SVEC-10 monolayer at different glucose concentrations. No significant changes were observed in the percentage of adherent monocytes/foam cells on the cell construct after 1 h incubation. Percentage of surface monocytes/foam cells B), transmigrated foam cells percentage C), and the non-foamy monocytes percentage D) in the total monocyte/foam cell count in the 3D-intimal model after 48 h incubation. No significant rise in these parameters was observed. Values are mean ± SD, $n = 3$, one-way ANOVA. *$p<0.05$, **$p< 0.01$, ns – not significant compared to the control. Microscopic images show the morphology of the adherent monocytes/foam cells on the cell construct and the transmigrated cells in all groups: E) euglycemia, F) moderate, G) high, and H) severe hyperglycemia.

and COX-2, was measured by western blot. The three major treatment groups: 25 mM glucose (severe hyperglycemia), 200 pg mL^{-1} LPS (chronic inflammation), and multi-disease condition (25 mM glucose+50 pg mL^{-1} LPS), were checked for inflammatory protein expression and compared with the control group (without additional glucose and LPS). IL-6 was not detected in our system. However, IL- 1β showed the most sensitivity in our system. There were no noticeable differences in IL- 1β secretion in severe hyperglycemia, but a significant enhancement in protein secretion was found in chronic inflammation and multi-disease conditions (**Figure** 8A). An almost 10-fold enhanced signal was recorded in both groups compared to the control. Interestingly, TNF-α was significantly expressed in severe glycemia while not substantial in chronic inflammation. A significance of $p<0.001$ was recorded in the multi-disease condition (Figure 8B). Moreover, all groups showed a non-significant expression profile for COX-2 in our system (Figure 8C). The chemiluminescent images showed the respective protein bands for all groups (Figure 8D).

3. Discussion

Atherosclerosis involves multi-step complexities and critical changes in the vessel layer. The blood vessel wall consists of three layers: intima, media, and adventitia. The intima comprises endothelium and subendothelial connective tissue and is separated from the media by the elastic lamina interna. In the early stage of atherosclerosis, endothelial dysfunction initiates the retention of lipoproteins bound to the ECM in the intima.[47] It leads to the passage of inflammatory cells, especially macrophages and T cells, into the arterial wall, followed by the migration and proliferation of VSMCs in the intimal layer.[48] In our study, we developed a disease-induced 3D hydrogel-based intimal model mimicking the early events of atherosclerosis. The intimal layer consisted of MOVAS-collagen constructs with a lining of SVEC-10 monolayer on the top of the construct. In our model, we added MOVAS in the collagen and allowed intimal thickening by prolonging the incubation period of MOVAS for 6 days. Atherosclerosis plaque formation is believed to be related to the aberrant proliferation of VSMCs in the intimal layer. Moreover, phenotypic alteration of VSMCs from contractile to synthetic phenotype in the atherosclerosis intima results in less expression of VSMC markers, and this alteration directly contributes to atherosclerosis.[49] In our model, MOVAS grew rapidly in the collagen construct after one day of incubation and maintained the cell viability/metabolic activity for 6 days (Figure S1, Supporting Information). The model also used native LDL (25 µg mL^{-1}) within the physiological range (<100 mg/dL) to promote transendothelial transfusion of LDL as an in vivo system.[50] The model could effectively retain the LDL transfusion in the intimal layer that subsequently accumulated in transmigrated monocytes, which allowed monocyte conversion to foam cells.

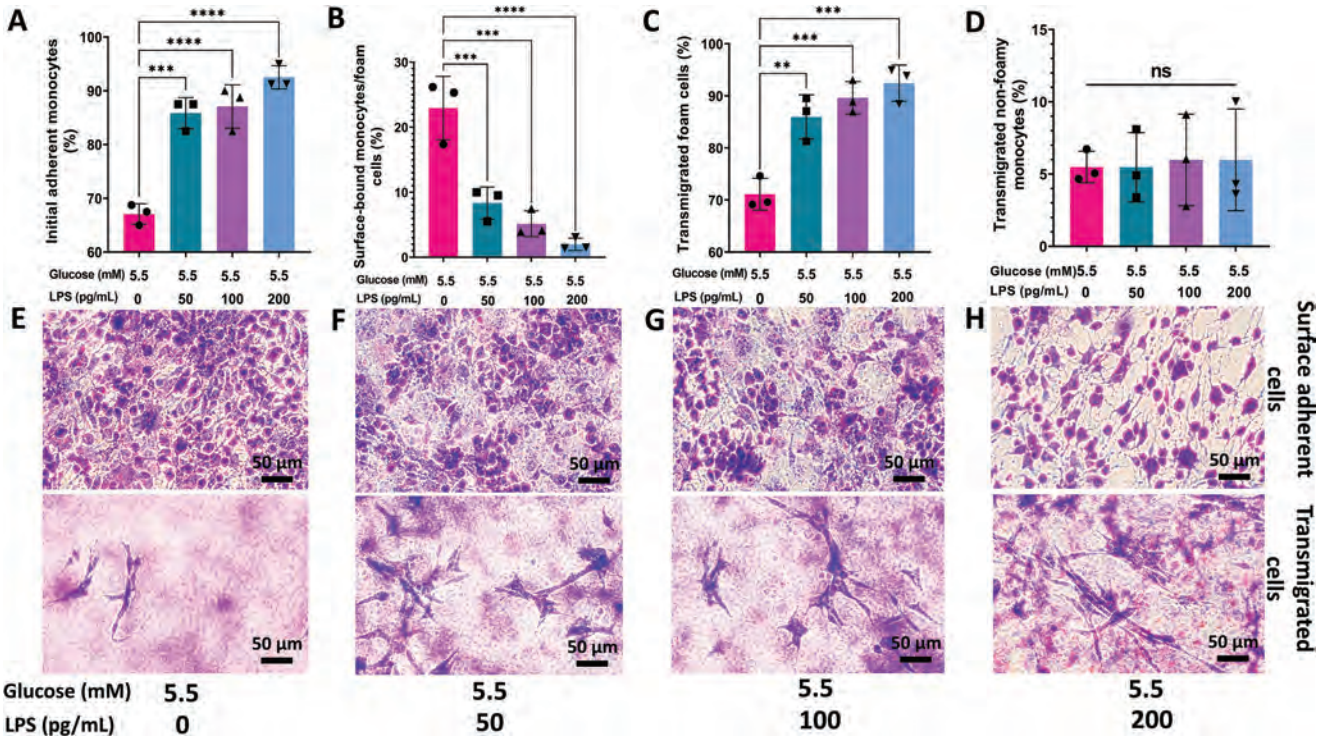

Figure 6. Influence of chronic infection in monocyte transmigration and foam cell formation in the 3D-atherosclerosis intimal model. A) Quantification of initial monocyte adhesion on the SVEC-10 monolayer in different LPS concentrations. A significant rise was observed in the percentage of adherent monocytes/foam cells on the cell construct after 1 h incubation in all treated groups. Percentage of surface-bound monocytes/foam cells B), percentage of transmigrated foam cells C), and percentage of non-foamy monocytes D) in the total monocyte/foam cell count in the 3D-intimal model after 48 h incubation. Values are mean ± SD, $n = 3$, one-way ANOVA. $^{**}p<0.01$, $^{***}p< 0.001$, $^{****}p< 0.0001$, ns – not significant compared to the control. Microscopic images show the morphology of the adherent monocytes/foam cells on the cell construct and the transmigrated cells in control E) 0 pg mL^{-1}, F) 50 pg mL^{-1}, G) 100 pg mL^{-1} and H) 200 pg mL^{-1} LPS treated groups.

Previous findings supported such LDL transfusion and retention in the hydrogel construct.[39,51] However, those studies employed higher concentrations of LDL (4 to 40 times higher) with more prolonged incubation in their systems than ours. Although the transportation of native LDL in the subendothelial space was not depicted in our model, it is likely to pass through the intercellular junctions under high glucose or infection stimulation.

The major producer of extracellular matrix within the vessel walls is the VSMC, which produces different matrix proteins in response to atherogenic stimuli.[40] The production of proteoglycans from VSMCs facilitates the intimal retention of lipoproteins.[52] Moreover, VSMCs within the intimal wall interact with transmigrating monocytes, contributing to their retention and function within the vasculature.[53] The addition of MOVAS in collagen construct showed promising improvement in lipid-laden foam cell formation in our atherosclerosis model. The MOVAS-embedded 3D-intimal model showed a significant increase in foam cell formation compared to the non-MOVAS model. Moreover, adding MOVAS to the collagen construct improved the cell migration distance in our model. Microscopic images clearly showed the increased number of foam cells attached at the bottom of the well (indicating that they migrated throughout the hydrogel construct) in the MOVAS embedded group than in that of no MOVAS. The red droplets confirmed the deposition of lipids in the cells (Figure 4). However, our study did not consider the smooth muscle-derived foam cell formation that might influence our model's total foam cell count.

The most important depiction of our system is to mimic the disease-induced microenvironment in evaluating the risk of multi-disease complexities in atherosclerosis plaque development. The direct influence of hyperglycemia in atherosclerosis plaque development is still not clear, while many studies showed the augmented expression of adhesion molecules such as intracellular adhesion molecule 1 (ICAM-1), vascular cell adhesion molecule-1 (VCAM-1) and monocyte chemoattractant protein-1 (MCP-1) in the diabetic endothelial, as well as activation of the PI3K/AKT/NF-κB signaling pathway in vitro and in vivo.[14,20,21,54–56] Our studies showed an incremental increase in monocyte adhesion to SVEC-10 monolayer in moderate (15 mM D-glucose), high (20 mM D-glucose), and severe (25 mM D- glucose) hyperglycemia. Similar results were reported in a previous study. The study mimicked gestational diabetes mellitus by adding 30 mM glucose that increased THP-1 cell adhesion to HUVEC. The study found the overexpression of Cx43 in HUVEC at high glucose conditions, activating the PI3K/AKT/NF-κB signaling and downstream expression of adhesion molecules, ultimately resulting in an increment in monocyte-endothelial adhesion.[55] Our findings also correlated with the in vivo studies. High glucose (25 mM) administration in rat mesenteric venules leads to increased immunoreactivity of P-selectin and

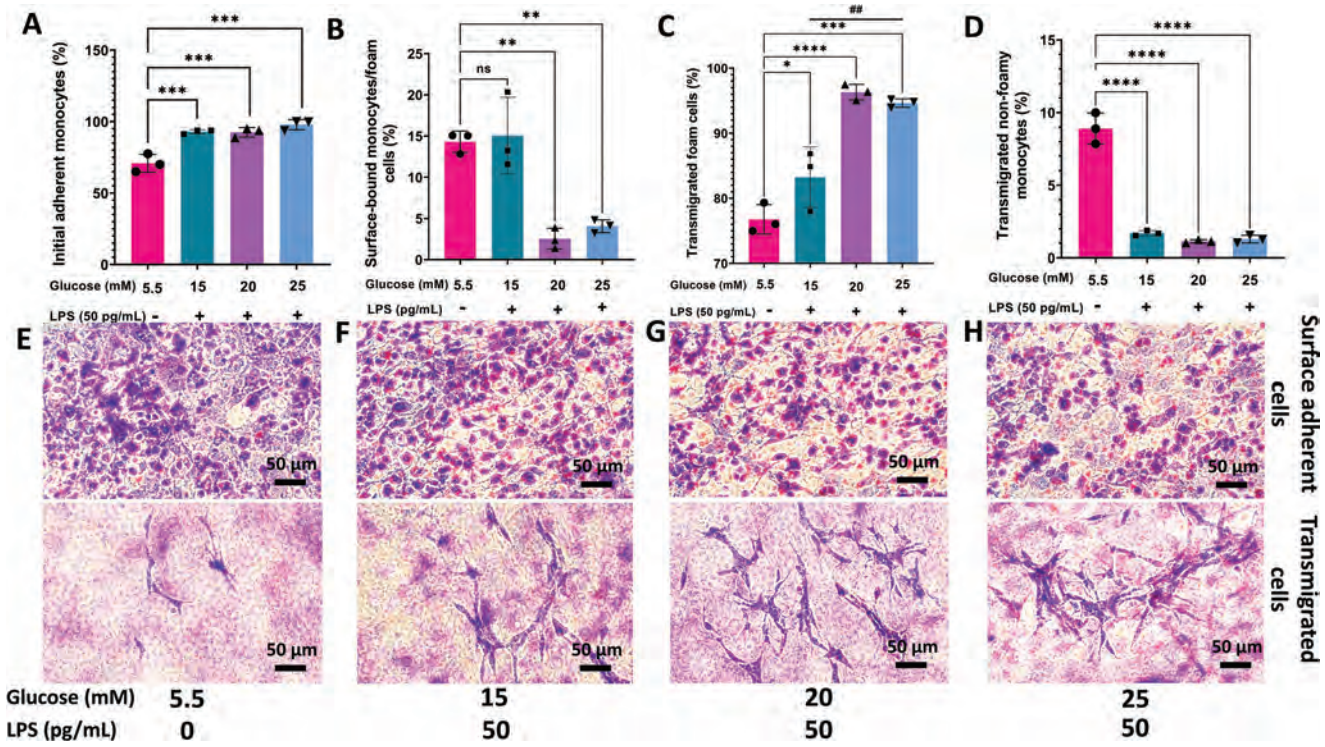

Figure 7. Monocyte transmigration and foam cell formation in a 3D intimal model in multi-disease complexities. A) Quantification of initial monocyte adhesion on SVEC-10 monolayer after 1 h incubation in multi-disease conditions. Percentage of surface-bound monocytes/foam cells B), percentage of transmigrated foam cells C), and percentage of non-foamy monocytes D) in total monocytes/foam cells in the 3D intimal model after 48 h incubation. Values are mean ± SD, $n = 3$, one-way ANOVA. *p<0.05, **p<0.01, ***p< 0.001, ****p<0.0001, ns – not significant compared to the control, ##p<0.01 compared to the 15 mM glucose+50 pg mL^{-1} LPS-treated group. E) Microscopic images show the morphology of the surface-bound monocytes/foam cells and the transmigrated cells in control (no additional glucose and LPS), F) 15 mM glucose+ LPS, G) 20 mM glucose+ LPS, and H) 25 mM glucose+ LPS treated groups.

ICAM-1, increasing inflammatory cell adhesion,[57] while CD44-deficient mice showed less monocyte infiltration in type-1 diabetic condition.[58] The monocyte transmigration in our model might correlate with the endothelial dysfunction caused by the treatment introduced in our model. Although the percentages of transmigrated foam cells and transmigrated non-foam cells in high glucose conditions were not statistically different from those in euglycemic conditions (5.5 mM) (Figure 7), the total adhered/transmigrated cells increased at high glucose conditions (Figure S4, Supporting Information). Particularly, adding 20 mM glucose significantly increased the total monocyte/foam cell number, including surface-bound and transmigrated monocytes/foam cells. However, a drastic decrease in total cell count was observed in the 25 mM glucose-treated group (Figure S4A,B, Supporting Information). The reason for cell death in our model is unknown. However, many types of cells are stressed by high glucose, forming oxidative and nitrosative species such as superoxide, nitric oxide, and peroxynitrite. These species play a role in diabetes-mediated cardiovascular complications induced by high glucose-mediated apoptotic cell death.[59] A similar pattern was observed in the dual disease conditions. The addition of LPS with glucose did not significantly increase the total cell count but reduced the cell number in the highest concentration-treated groups (Figure S4E,F, Supporting Information), while LPS-treated groups showed an increment in total cell count in a dose-dependent manner (Figure S4C,D, Supporting Information).

LPS-induced 3D-atherosclerosis model showed the potential to mimic in vivo relevant chronic infection. LPS is a potent monocyte/macrophage stimulator that can induce the production of inflammatory cytokines and chemokines.[60] Studies also find that LPS induces macrophage-derived foam cells, leading to atherosclerotic plaque development in vitro and in vivo.[61] There is evidence that LPS induces autophagy in macrophages, suggesting that autophagy contributes to forming foam cells in response to LPS.[61,62] In our model, the addition of LPS significantly increases monocyte attachment and transmigration in a dose-dependent pattern. The initial monocyte adhesion was enhanced by ~30% in the treated groups compared to the control. Approximately 90–95% of the transmigrated cells converted to foam cells, which was significantly higher than that in the control (p<0.001), while no remarkable difference was observed among the doses. The immunofluorescence images also supported the finding. The dysfunctional endothelial monolayer upon LPS stimulation might induce monocyte transmigration in our system. Furthermore, multi-disease conditions achieved by adding glucose and LPS extended the importance of our model to identify patient-specific atherosclerosis risk. The addition of a small dose of LPS (50 pg mL^{-1}) with glucose showed enhancement in cell transmigration and foam cell formation. Glucose alone was not a strong

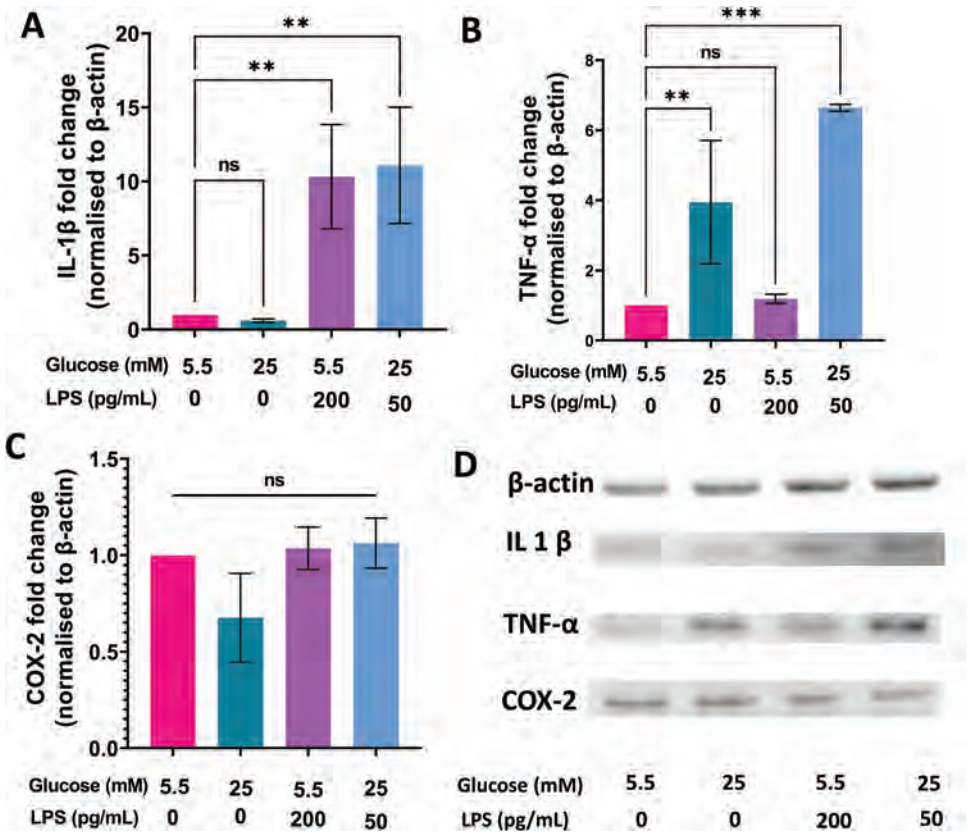

Figure 8. Inflammatory protein secretion profile from the Glucose and LPS-stimulated 3D-intimal model. A) IL-1 β, B) TNF-α, and C) COX-2 secretion from severe hyperglycemia, chronic infection, and muti-disease stimulated 3D-atherosclerosis intimal model. Graphs showed representative protein levels normalized to housekeeping protein β-actin. Values are mean ± SD, $n = 3$, one-way ANOVA. $^{**}p<0.01$, $^{***}p< 0.001$, ns – not significant compared to the control D) Chemiluminescent images of respective proteins and β-actin housekeeping protein.

mediator for foam cell transformation in our system while adding LPS increased foam cell formation compared to the control in all doses. There were also significant differences among doses. The percentages of foam cells in the LPS+20 mM glucose and LPS+25 mM glucose groups were significantly higher ($p<0.01$) than that in the LPS+15 mM glucose group (Figure 7C). LPS with glucose might synergistically mediate endothelial dysfunction and monocyte activation, increasing monocyte transmigration and foam cell formation.

Finally, we checked the expression of different inflammatory biomarkers in various disease conditions. Different inflammatory cytokines predominated in different disease states. TNF-α secretion was ~4 and ~6.5 times higher in severe hyperglycemia (25 mM glucose) and multi-disease states (25 mM glucose + 50 pg mL^{-1} LPS), respectively, than that in the control, while no remarkable increase was observed in chronic infection (200 pg mL^{-1} LPS). The LPS played a pivotal role in IL-1β secretion in our model. There was increased expression of IL-1β in the LPS-treated group but not in the glucose-treated group. However, the increased secretion of IL-1β was recorded after adding LPS to the glucose. The result is supported by Dissanayake et. al.[63] The study investigated the potential role of α-E catenin in the polarization of macrophages in high glucose conditions (25 mM). The study suggested the direct influence of LPS stimulation on glucose-induced IL-1β secretion, but no changes in TNF-α expression. However, the inflammatory protein secretion was somehow time and dose-dependent. The addition of 15 mM glucose in THP-1 cells for 48 h showed a maximum increase in IL-1β than euglycemic and hyperglycemic conditions (20 and 25 mM) treated for 72 h, mediated by PKC-alpha, via phosphorylation of p38 MAPK and ERK1/2 leading to NF-kappaB activation.[64] Moreover, hyperglycemia suppresses CD33 expression and triggers the spontaneous secretion of TNF-α by peripheral monocytes.[65] In our study, while the monocyte adhesion and transmigration were tested in different conditions and concentrations of glucose and LPS, we only checked the inflammatory protein secretion in four treatment groups: euglycemia (5.5 mM glucose), severe hyperglycemia (25 mM glucose), chronic infection (200 pg mL^{-1} LPS), and severe hypoglycemia-infection (25 mM glucose+50 pg mL^{-1} LPS). It might be useful to check the protein expression profile in all treatment conditions similar to the monocyte studies to correlate the data between experiments.

4. Conclusion, Limitation and Future Direction

Overall, the in vitro disease-induced 3D-atherosclerosis model described here is suitable for mimicking the early atherosclerosis event in multi-disease complexities. We evaluated early events of atherosclerosis in our model, including monocyte adhe-

sion, transmigration, and foam cell formation amongst different treated groups, and successfully emulated atherosclerosis risk in different disease conditions in our model. Most importantly, the model achieved subendothelial transfusion and accumulation of native LDL, which then induced foam cell formation within the intimal layer similar to physiological conditions. The findings obtained from this model in different disease-relevant conditions correlate well with those in the reported in vitro and in vivo studies, proving the model's accuracy. Our model could be useful to study the risk of atherosclerosis development in different disease conditions. Finally, this model might be beneficial to study cellular crosstalk in the atherogenesis process to understand the biochemical mechanism involved in plaque formation and be used to test new drugs by targeting patient-specific mechanisms.

Although the model provides a unique platform for developing in vitro disease-induced conditions to evaluate early atherosclerosis risk, several limitations should be addressed in the future. In the current study, we did not check the phenotypic variation of MOVAS in our model. It is imperative to know whether the phenotypic alteration has occurred to mimic the atherosclerosis intima. VSMCs in the atherosclerotic intima reduced contractility due to their dedifferentiated or synthetic nature. The expression of α-smooth muscle actin (α-SMA) is considered a crucial biomarker for confirming the phenotypic alteration of VSMC in atherosclerosis. In addition, we did not check the expression level of adhesion molecules such as VCAM, ICAM, and MCP-1 in different disease groups, which might better explain the variation in the initial monocyte adhesion in our model in different treated groups. Another limitation of our study is that we did not consider the MOVAS-derived foam cell formation. It has been suggested that VSMCs comprise at least 50% of the foam cells in atheroma lesions in humans. The role of each cell type must be determined, which requires the identification of the factors and mechanisms regulating the phenotypic transition of VSMCs and monocytes/macrophages, as well as an understanding of how these phenotypically modulated cells contribute to disease development. In future studies, cell-specific biomarker secretion in different disease conditions could be conducted to evaluate individual risks in plaque development. The model could be employed as a live imaging platform using cell-specific fluorescence dye to investigate the different steps of plaque development in multiple disease conditions. Moreover, in the future, we aim to use patient-derived cell lines to replicate patient-specific pathophysiological microenvironment and introduce hemodynamic conditions to achieve physiological accuracy to study mechanobiology and extend the use of the model for patient-specific therapeutic development.

5. Experimental Section

Cell Culture: This study used SVEC4-10 (a murine endothelial cell line), MOVAS (a murine aortic smooth muscle cell), and RAW 264.7 (murine monocytes/macrophage-like cells) from ATCC, Rockville, MD. The cells were grown in DMEM (Dulbecco's Modified Eagle Medium) low glucose (5.5 mM) medium supplemented with 100 IU mL^{-1} of penicillin G, 100 µg mL^{-1} streptomycin, and 10% (v/v) FBS, at 37 °C in a humidified atmosphere, with 5% of CO_2. SVEC-10 and MOVAS were used within passage number 5–8.

Experimental Parameters for Disease-Induced Atherosclerosis Model: To determine the optimal treatment time for each disease condition, such as hyperglycemia and chronic infection, all cell lines, including SVEC-10, MOVAS, and RAW 264.7, were treated with different glucose concentrations (15 mM, 20 mM, 25 mM and 30 mM D-glucose) and LPS concentrations (50 pg mL^{-1}, 100 pg mL^{-1}, 200 pg mL^{-1}, and 1 ng mL^{-1}) for 24 h and checked the cell viability/metabolic activity at different time points. SVEC-10 and MOVAS cells were seeded in 96-well plates at a concentration of 10000 cells per well and incubated overnight for confluent monolayer formation. On the other hand, RAW 264.7 cells were seeded at a concentration of 20000 cells per well and incubated overnight before treatment. After overnight incubation, the media was taken out from each well and was replenished with new cell culture media containing additional glucose or LPS to mimic hyperglycaemic and infectious conditions. Each group included a control without any additional treatments. Presto blue assay was used to determine cell viability. A 1:10 dilution of presto blue solution in PBS was added in each well, then incubated in a 37 °C 5% CO_2 incubator for 20 min before reading the results. A plate reader was used to measure absorbance at 570 nm.

5.0.0.1. Construction of Intimal Model: 3D collagen-MOVAS constructs were prepared using type-1 rat tail collagen (R&D Biosystems). MOVAS was cultured in a flask and trypsinized when confluent. Collagen constructs were prepared with varying concentrations of MOVAS ranging from 2500-10000 cells per well and checked the cell viability/metabolic activity at different time points. Briefly, 1 mL of 2 mg mL^{-1} collagen hydrogel precursor solution was prepared by adding 400 µL collagen stock (5 mg mL^{-1}) solution to 100 µL of 10X low glucose DMEM (without FBS and pen-strep) and neutralized by 1N sterile NaOH (~21 µL). MOVAS suspension and deionized (DI) water were added to the above collagen solution to reach a final volume of up to 1 mL. A 50 µL of MOVAS-collagen precursor mixture was pipetted into a well in 96-well plates and incubated for an hour in the cell incubator (5% CO_2, 37 °C) to polymerize the gel. The rapid growth in viability/metabolic activity was observed in the collagen construct containing 5000 cells and maintained the activity up to 6 days of incubation. Collagen construct with 2500, 7500, and 10000 cells also maintained good viability/metabolic activity but started to reduce slightly at day 6 (Figure S1, Supporting Information). Therefore, the MOVAS concentration used in our model was decided to be 5000 cells per well. The final thickness of the collagen construct was ≈1 mm. Finally, SVEC4-10 was seeded on the top of the MOVAS-collagen construct at a concentration of 20000 cells per well. The cells were cultured for 6 days to get a compact endothelial monolayer on the top of the MOVAS-collagen construct and also allowed MOVAS proliferation in matrix deposition in the hydrogel construct.

Confirmation of Endothelial Integrity by Immunostaining: The media was removed from the coculture model and rinsed thrice with PBS, and then 100 µl of 4% paraformaldehyde (PFA) was added for an hour to fix the cells. The samples were stored at 4 °C until imaging. The endothelial junction integrity on the top of the collagen-MOVAS construct was detected using Alexa FluorTM 488 conjugated anti-Mo CD144 (VE-cadherin) monoclonal antibody. A 1:100 dilution of the antibody was prepared in PBS. To perform this staining, the 4% PFA was removed from the well, rinsed with PBS, and blocked with 1% BSA in PBS for an hour at 4 °C. The blocking agent was washed with PBS twice, and 100 µl of dye-conjugated monoclonal antibody was added and incubated at 4 °C for 2 h. The collagen construct was extensively washed with PBS to remove the excess dye from the gel. A 21 G needle was used to rim the edges of the gels, placed the construct in a small petri dish containing 5 mL of PBS for 15 min, and changed the PBS four times, followed by 15 min of washing each time. The coculture construct was then placed on a glass slide. A cover slip was placed over the coculture construct, and the slide was mounted to take the images. Images were acquired using a confocal microscope (Olympus FV3000RS NIR) and processed using Fiji ImageJ.

Confirmation of Endothelial Integrity by Tetramethylrhodamine Isothiocyanate (TRITC)-Dextran Permeability Assay: The endothelial cells were grown on the top of the MOVAS-collage construct for 6 days to get the confluent monolayer. Each construct was washed with 1x PBS once. A 100 µl of TRITC-dextran (0.5 mg mL^{-1}) solution in media was added to each well and incubated for 30 min at room temperature. After incubation,

the TRITC-dextran solution was removed, and each construct was washed thrice with 1x PBS. A 100 µl of collagenase-D (2.5 mg mL^{-1}) solution was added to each well and incubated for 15 min at 37 °C to digest the coculture construct. The level of permeability of the TRITC-dextran was quantified through the measurement of fluorescence intensity using a plate reader at 550 nm excitation and 570 nm emission wavelength.

Low-Density Lipoprotein Isolation Technique from Whole Blood: The low-density lipoprotein (LDL) was separated from whole blood serum using potassium bromide density gradient ultracentrifugation, followed by slightly modified previous protocols.[42] A whole blood sample was collected from the Red Cross (Griffith University Human Ethics Committee, approval number 2021/598) and centrifuged for 10 min at 2000 x g to remove red and white blood cells, and the supernatant was collected. Additional centrifugation at 10 000 × g for 30 min was performed to remove the platelets, supernatant was collected. Plasma solvent density was adjusted by KBr to achieve 1.063 g mL^{-1}, using the following formula:

$$\text{Amount of KBr added (g)} = \text{Volume of Plasma (mL)} \times 0.0834 \quad (1)$$

The density-adjusted plasma solution was added in a 38.5 thin wall ultra-clear polycarbonate tube. The plasma was centrifuged for 24 h at 40 000 rpm at 4 °C, using a 70 Ti rotor (Optima XPN-90 Ultracentrifuge). After 24 h of centrifugation, the supernatants were removed, and the LDL-rich layer separated by density gradient was collected. LDL was then dialyzed against PBS (pH-7.4) for 24 h, with PBS changed every 6 h. LDL was stored at −20 °C and used within 4 weeks. The protein concentration was checked by standard BCA (Bicinchoninic Acid) protein assay following manufacturer instructions. Finally, the isolation of LDL was confirmed by SDS-PAGE electrophoresis (Figure S2, Supporting Information).

Influence of Vascular Smooth Muscle Cells on Monocyte Transmigration and Foam Cell Conversion: This section investigated the effect of MOVAS on monocyte transmigration and, ultimately, foam cell formation. For this study, two different collagen constructs were made: with or without MOVAS. A 2 mg mL^{-1} collagen solution with MOVAS was prepared from 5 mg mL^{-1} rat tail collagen stock according to the abovementioned procedures, and 50 µL of the neutralized solution was added in each well of a 96-well plate. A 2 mg mL^{-1} neutralized collagen precursor solution without MOVAS was also added to the 96 well to get the only collagen hydrogel. Both groups were kept at 37 °C, a 5% CO_2 humid environment, for an hour for gel polymerization. SVEC-10 cells were seeded at 20000 cells per well on both constructs (with or without MOVAS) and allowed to grow for 6 days to achieve tight junction integrity. The media was changed every day for 6 days. The models were treated with 10 ng mL^{-1} TNF-α and 25 µg mL^{-1} LDL to induce endothelial dysfunction and monocyte adhesion. The treated media was removed, the construct was washed twice with PBS, and monocytes were then added at 20000 cells per well. The monocytes were incubated for an hour, media was collected from each well, and the construct was washed twice with cell culture media to collect all non-adherent cells. A hemocytometer was used to count non-adherent cells. The adherent cells were calculated by subtracting the non-adherent cells from the total added monocytes in each well. The adherent cell percentage was then calculated based on the total monocytes added. The following equation was used to calculate the percentage.

$$\text{Inherent adherent monocyte (\%)} = \frac{\text{Adherent cells in one well}}{20000} \times 100 \quad (2)$$

The co-culture models were replenished with fresh media and incubated for 48 h to allow cell transmigration and foam cell formation.

Transmigration of Monocytes and Foam Cell Formation in Hyperglycaemic Condition: After SVEC-10 monolayers were grown to confluence, the intimal models were treated for 8 h with 5.5, 15, 20, and 25 mM D-glucose along with 25 µg mL^{-1} native-LDL to imitate euglycaemic (control), moderate, high, and severe hyperglycaemic conditions. Euglycaemia or the control group was achieved using low-glucose DMEM media, while hyperglycaemic conditions required additional glucose levels, which were adjusted with D-glucose in the same media. Monocytes (RAW 264.7 cells) were treated in a separate plate with different glucose concentrations for 8 h without additional LDL. Glucose and LDL-containing media were removed from the coculture samples after 8 h incubation, washed twice with PBS, and treated monocytes were then added at 20000 cells per well in the respective coculture model. The initial adherent cells were counted as described above. The intimal model was incubated for 48 h to allow the transmigration of monocytes and subsequent foam cell formation. The media was replenished every 24 h.

Monocyte Transmigration and Foam Cell Formation in Infectious Condition: The culture media were supplemented with lipopolysaccharide (LPS) to mimic the in vitro infectious condition. The effect of infection on monocyte kinetics in atherosclerosis was assessed with LPS concentrations of 50, 100, and 200 pg mL^{-1} in intimal models, along with 25 g mL^{-1} LDL for 8 h. A control was prepared without LPS to compare the data. The monocytes were treated with LPS at different concentrations but without additional LDL for the same period as the intimal model. The treated monocytes at a concentration of 20000 cells per well were seeded on top of the construct. The intimal models were replenished with fresh media and incubated for 48 h to allow cell transmigration and foam cell formation. The number of initial adherent monocytes, transmigrating cells, and foam cells were counted as mentioned above.

Monocyte Transmigration and Foam Cell Formation in Multi-Disease Conditions: The intimal models were treated with D-glucose and LPS to mimic both hyperglycemia and infection to investigate the multi-disease complexities in early atherosclerosis. The 3D-intimal coculture models were treated with 15, 20, and 25 mM D-glucose along with 50 pg mL^{-1} LPS and 25 µg mL^{-1} LDL for 8 h. A control without any addition of D-glucose and LPS was included. Monocytes were treated in similar disease complexities for 8 h but without LDL and added to the respective treated model. The number of initial adherent monocytes, transmigrating cells, and foam cells were counted as mentioned above.

Giemsa and Oil-Red-O Staining for Confirming Foam Cell Formation in the Intimal Model: Giemsa and oil-red-o staining were used to confirm the transmigrated monocytes and deposition of lipids in the foam cells in our intimal model. The monocytes were incubated for 48 h to allow the transmigration and conversion into foam cells. After 2 days of incubation, the intimal models were washed with PBS twice, and 4% PFA was added for an hour at room temperature (RT) for fixation. The model could be stored at 4°C until use. Monocyte and foam cell staining in the intimal model was performed by the previously described protocol with slight modification.[36] For oil-red-o staining, 4% PFA was removed from the intimal models and washed them with 50% methanol for 5 min. The model was then incubated for 15 min with 78% methanol, followed by the incubation with 0.2% freshly prepared oil-red-o solution for an hour at RT. The excess dye from the gel was washed 4 times with 78% methanol. The model was counterstained with Giemsa dye for 10 min at RT and washed once with deionized water. This staining method specifically stained the surface-bound and transmigrated monocytes/foam cells in the intimal model. No endothelial or MOVAS staining was detected in the intimal model (Figure S3, Supporting Information). The intimal coculture construct was removed from the well as described above, placed on a glass slide, and covered with a cover slip. The mounted slides were used to take the brightfield images using an inverted microscope (CKX53, Olympus) mounted with a digital camera (DP74, Olympus). The microscope's focus was adjusted to scroll down the intimal construct and the images of the cells to confirm the transmigration and conversion of the foam cells in the model. Cells were scored as either foam cells that showed the accumulation of lipid droplets in the cell cytoplasm in red color, or macrophages without any lipid accumulation with distinct dark purple/bluish purple cytoplasm.[35,36]

Quantification of Transmigrated Monocytes and Foam Cells: Quantifying transmigrated monocytes and foam cells in the intimal models was achieved in multiple steps. The first step was to collect the non-transmigrated monocytes/foam cells attaching to the SVEC-10 monolayer of the intimal model. After 48 h incubation, the media was aspirated, and the model was washed twice with PBS. The surface-bound monocyte/foam cells were de-attached by Trypsin and collected in a 1.5 mL vial. The trypsinized cell mixture was centrifuged at 300 ×g for 5 min and the cell pellet was resuspended in 100 µL fresh media. This group of samples was marked as set 1. To collect the transmigrated cells,

the coculture construct was digested by adding 100 µL (2.5 mg mL^{-1}) collagenase-D in each well.[43] The coculture model with collagenase-D was incubated at 37 °C for 20 min in an incubator, pipetted to mix well, and incubated for another 25 min to ensure complete digestion. A 100 µl of FBS-containing DMEM low glucose medium was added to each well to inhibit the enzyme's action, and the suspension was collected in a 1.5 mL vial. The cells attaching to the bottom of the well were collected by adding 30 µL of trypsin to each well, followed by 5 min incubation at 37 °C and 60 µL of culture media addition to neutralize the trypsin and collected into the prior vial. The mixture was centrifuged at 300 ×g for 5 min, the supernatant was discarded, and the cell pellet was resuspended in 300 µL fresh media. This group of samples was marked as set 2. Samples collected from sets 1 and 2 were diluted 10 times with cell media. A 5 µl suspension from the diluted sample was pipetted on a glass slide, making a thin smear. The slides for all samples were air-dried for 20 min at RT and blow-dried with a dryer for 10 s. The slides were then fixed with 4% PFA for 15 min and 78% methanol for another 15 min. A 500 µL of 0.2% oil-red-o stain solution was added to each slide and incubated for 15 min for lipid staining. The slides were washed with 78% methanol twice, then counterstained with Giemsa for 1 min for monocyte staining and washed with distilled water. The previously mentioned microscope and imaging software were used to take the brightfield images. Foam cells were identified by the accumulation of lipid droplets in the cell cytoplasm. The foam cells appeared in light pink/purple cytoplasm with red/orange lipid droplets with a foamy morphology. The non-foamy monocytes were determined by distinct deep purple/bluish purple cytoplasm without any lipid accumulation. The obtained data was quantified as follows:

$$1.\ \text{Surface} - \text{bound monocytes or foam cell}\ (\%) = \frac{\text{Number of monocytes and foam cells attached to the SVEC monolayer}}{\text{Total monocytes and foam cells in the intimal model (surface bound} + \text{transmigrated)}} \times 100 \quad (3)$$

$$2.\ \text{Transmigrated foam cells}\ (\%) = \frac{\text{Number of transmigrated foam cells}}{\text{Total monocytes and foam cells in the intimal model (surface bound} + \text{transmigrated)}} \times 100 \quad (4)$$

$$3.\ \text{Transmigrated nonfoamy monocytes}\ (\%) = \frac{\text{Number of transmigrated nonfoamy monocytes}}{\text{Total monocytes and foam cells in the intimal model (surface bound} + \text{transmigrated)}} \times 100 \quad (5)$$

Western Blot For Analyzing Protein Expression Profile: It has been reported that various inflammatory biomarkers were associated with atherosclerosis risk assessment.[44] Elevated inflammatory biomarkers in serum, including cytokines such as interleukins (IL)−1 and IL-6, IL-1β, IL-10, C-reactive protein (CRP), TNF-α, and PTX3, were commonly associated with atherosclerosis.[45] The expression of inflammatory biomarkers such as IL-6, IL-1β, TNF-α, and COX-2 was checked in different treated groups by western blotting. The protein extraction from the intimal model was followed by Alsharabasy et al.[43] with slight modification. Ten cell constructs were used for each treated group to collect the protein for western blot analysis. The media was discarded from the models and washed with 150 µL of PBS twice for 30 s each. As described above, the coculture model was digested with 100 µL of 2.5 mg mL^{-1} collagenase D. After digestion, the samples were centrifuged at 300 x *g* for 5 min at 4 °C, and supernatants were discarded. Next, the protein extraction was done as follows: i) kept the samples on ice for 10 min, ii) washed the cell pellets twice with 500 µL of cold PBS, centrifuged at 300 x g at 4 °C for 5 min, and discarded the supernatant. iii) added 30 µL of lysis buffer to each pellet, vortexed for 30 sec and incubated on ice for 20 min, iv) centrifuged the sample at 15 000 × *g* for 15 min at 4 °C, v) finally, transferred the supernatant into a pre-cooled eppendorf tubes and subjected to use for western blotting. The extracted protein concentration was measured using a micro-BCA assay kit and a sample with ≈40 µg protein was loaded, and then separated through 12.5% SDS-PAGE gel and transferred onto a PVDF membrane (Millipore).[46] The PVDF membranes were probed with anti-IL-6 (1:1000), anti-IL 1β (1:1000), anti-TNF-α (1:1000), and anti-COX-2 (1:1000) primary antibodies in 5% skim milk overnight at 4 °C. Membranes were washed and incubated with their corresponding secondary antibodies anti-rabbit HRP at room temperature for 1 h and imaged by chemiluminescence using a Sapphire biomolecular imager (Azure biosystem). Band intensity was measured using ImageJ and normalized to the housekeeping protein, β-actin (1:2500).

Statistical Analysis: Data representation was mean ± standard deviation (SD) of three independent experiments. T-test and one-way ANOVA were used to analyze the significant differences. A *p*-value of ≤0.05 was considered significant. Graphs were plotted using GraphPad Prism 9.

Supporting Information

Supporting Information is available from the Wiley Online Library or from the author.

Acknowledgements

This work is funded by the National Health and Medical Research Council (HTT: APP1146694, APP1182347, APP2002827) and the Heart Foundation (HTT: 102761). The authors would like to acknowledge the Australian National Fabrication Facility (Queensland Node) for access to key items of equipment.

Open access publishing facilitated by Griffith University, as part of the Wiley - Griffith University agreement via the Council of Australian University Librarians.

Conflict of Interest

The authors declare no conflict of interest.

Data Availability Statement

The data that support the findings of this study are available from the corresponding author upon reasonable request.

Keywords

atherosclerosis 3D-coculture, foam cells, hyperglycemia, infections, transmigration

Received: August 30, 2023
Revised: December 19, 2023
Published online:

[1] D. Tschoepe, *Diabet. Res. Clinic. Pract.* **1996**, *30*, S19.
[2] J. P. Mauldin, S. Srinivasan, A. Mulya, A. Gebre, J. S. Parks, A. Daugherty, C. C. Hedrick, *J. Biol. Chem.* **2006**, *281*, 21216.
[3] S. L. Ullevig, Q. Zhao, D. Zamora, R. Asmis, *Atherosclerosis* **2011**, *219*, 409.
[4] K. X. Vazquez-Prada, J. Lam, D. Kamato, Z. P. Xu, P. J. Little, H. T. Ta, *Arterioscler. Thromb. Vasc. Biol.* **2021**, *41*, 601.
[5] F. Akther, J. Zhang, H. D. N. Tran, H. Fallahi, H. Adelnia, H. P. Phan, N. T. Nguyen, H. T. Ta, *Adv. Biol.* **2022**, *6*, 2101316.
[6] B. Perera, Y. Wu, N. T. Nguyen, H. T. Ta, *Mater. Today Bio.* **2023**, *22*, 100767.
[7] C. L. V. Westhorpe, E. M. Dufour, A. Maisa, A. Jaworowski, S. M. Crowe, W. A. Muller, *Exp. Mol. Pathol.* **2012**, *93*, 220.
[8] Y. Wu, K. X. Vazquez-Prada, Y. Liu, A. K. Whittaker, R. Zhang, H. T. Ta, *Nanotheranostics* **2021**, *5*, 499.
[9] J. R. Pickett, Y. Wu, L. F. Zacchi, H. T. Ta, *Cardiovasc. Res.* **2023**, *119*, 2278.
[10] H. T. Ta, N. P. Truong, A. K. Whittaker, T. P. Davis, K. Peter, *Exp. Opinion Drug Del.* **2018**, *15*, 33.
[11] Y. Zhang, A. Koradia, D. Kamato, A. Popat, P. J. Little, H. T. Ta, *J. Pharm. Pharmacol.* **2019**, *71*, 1029.
[12] A. Zia, Y. Wu, T. Nguyen, X. Wang, K. Peter, H. T. Ta, *Cardiovasc. Res.* **2020**, *116*, 2055.
[13] I. Tabas, A. H. Lichtman, *Immunity* **2017**, *47*, 621.
[14] R. Piga, Y. Naito, S. Kokura, O. Handa, T. Yoshikawa, *Atherosclerosis* **2007**, *193*, 328.
[15] L. A. Campbell, M. E. Rosenfeld, *Arch Med. Res.* **2015**, *46*, 339.
[16] S. R. Kashyap, L. J. Roman, J. Lamont, B. S. S. Masters, M. Bajaj, S. Suraamornkul, R. Belfort, R. Berria, D. L. Kellogg, J. Y. Liu, R. A. DeFronzo, *J. Clin. Endocrinol. Metab.* **2005**, *90*, 1100.
[17] S. M. Haffner, S. Lehto, T. Rönnemaa, K. Pyörälä, M. Laakso, *N. Engl. J. Med.* **1998**, *339*, 229.
[18] D. Aronson, E. J. Rayfield, *Cardiovasc. Diabetol.* **2002**, *1*, 1.
[19] T. Altannavch, K. Roubalová, P. Kucera, M. Andel, *Physiol Res* **2004**, *53*, 77.
[20] A. M. Schmidt, O. Hori, J. X. Chen, J. F. Li, J. Crandall, J. Zhang, R. Cao, S. D. Yan, J. Brett, D. Stern, *J. Clin. Invest.* **1995**, *96*, 1395.
[21] A. Otsuka, K. Azuma, T. Iesaki, F. Sato, T. Hirose, T. Shimizu, Y. Tanaka, H. Daida, R. Kawamori, H. Watada, *Diabetologia* **2005**, *48*, 2667.
[22] L. A. Campbell, M. E. Rosenfeld, *Arch. Med. Res.* **2015**, *46*, 339.
[23] M. E. Rosenfeld, L. A. Campbell, *Thromb Haemost* **2011**, *106*, 858.
[24] A. M. Gorabi, N. Kiaie, A. Khosrojerdi, T. Jamialahmadi, K. Al-Rasadi, T. P. Johnston, A. Sahebkar, *Tren. Cardiovasc. Medi.* **2022**, *32*, 525.
[25] I. Sieve, M. Ricke-Hoch, M. Kasten, K. Battmer, B. Stapel, C. S. Falk, M. S. Leisegang, A. Haverich, M. Scherr, D. Hilfiker-Kleiner, *Vasc. Pharmacol.* **2018**, *103–105*, 16.
[26] C. R. H. Raetz, C. Whitfield, *Annu. Rev. Biochem.* **2002**, *71*, 635.
[27] M. Inoue, T. Ishida, T. Yasuda, R. Toh, T. Hara, H. M. Cangara, Y. Rikitake, K. Taira, L.i Sun, R. K. Kundu, T. Quertermous, K. I. Hirata, *Microvasc. Res.* **2010**, *80*, 179.
[28] T. Keiper, N. Al-Fakhri, E. Chavakis, A. N. Athanasopoulos, B. Isermann, S. Herzog, R. Saffrich, K. Hersemeyer, R. M. Bohle, J. Haendeler, K. T. Preissner, S. Santoso, T. Chavakis, *FASEB J.* **2005**, *19*, 2078.
[29] M. Klouche, A. E. May, M. Hemmes, M. MeBner, S. M. Kanse, K. T. Preissner, S. Bhakdi, *Arterioscler. Thromb. Vasc. Biol.* **1999**, *19*, 784.
[30] J. M. Murphy, K. Jeong, Y. A. R. Rodriguez, J. H. Kim, E. E. Ahn, S. S. Lim, *Sci Rep* **2019**, *9*, 7617.
[31] S. Ramachandran, A. Vinitha, C. C. Kartha, *Cardiovasc. Diabetol.* **2016**, *15*, 152.
[32] C. A. Gleissner, N. Leitinger, K. Ley, *Hypertension* **2007**, *50*, 276.
[33] W. A. Muller, S. A. Weigl, *J. Exp. Med.* **1992**, *176*, 819.
[34] D. Nandy, R. Janardhanan, D. Mukhopadhyay, A. Basu, *J. Investig. Med.* **2011**, *59*, 661.
[35] T. A. Angelovich, M. D. Y. Shi, J. Zhou, A. Maisa, A. C. Hearps, A. Jaworowski, *Exp. Gerontol.* **2016**, *80*, 17.
[36] T. A. Angelovich, A. C. Hearps, A. Maisa, T. Kelesidis, A. Jaworowski, *J Vis Exp* **2017**, *2017*, e56293.
[37] T. A. Angelovich, A. C. Hearps, M. N. Oda, M. S. Borja, D. Huynh, S. Homann, A. Jaworowski, T. Kelesidis, *Aids* **2017**, *31*, 2331.
[38] A. Garcia-Sabaté, W. K. E. Mohamed, J. Sapudom, A. Alatoom, L. Al Safadi, J. C. M. Teo, *Bioengineering* **2020**, *7*, 113.
[39] M. Liu, S. Samant, C. H. Vasa, R. M. Pedrigi, U. M. Oguz, S. Ryu, T. Wei, D. R. Anderson, D. K. Agrawal, Y. S. Chatzizisis, *PLoS One* **2023**, *18*, e0280385.
[40] A. C. Doran, N. Meller, C. A. McNamara, *Arterioscler. Thromb. Vasc. Biol.* **2008**, *28*, 812.
[41] G. Song, C. Zheng, Y. Liu, M. Ding, P. Liu, J. Xu, W. Wang, J. Wang, *Mater. Des.* **2021**, *199*, 109428.
[42] D. W. Morel, J. R. Hessler, G. M. Chisolm, *J. Lipid Res.* **1983**, *24*, 1070.
[43] A. M. Alsharabasy, A. Pandit, *STAR Protoc.* **2021**, *2*, 100387.
[44] L. Z. Hong, Q. Xue, H. Shao, *J Inflamm Res* **2021**, *14*, 379.
[45] A. Shindo, H. Tanemura, K. Yata, K. Hamada, M. Shibata, Y. Umeda, F. Asakura, N. Toma, H. Sakaida, T. Fujisawa, W. Taki, H. Tomimoto, *PLoS One* **2014**, *9*, e100045.
[46] Y. Wu, G. Cowin, S. S. Moonshi, H. D. N. Tran, N. A. Fithri, A. K. Whittaker, R. Zhang, H. T. Ta, *Mater. Sci. Eng., C* **2021**, *131*, 112477.
[47] Y. Nakashima, H. Fujii, S. Sumiyoshi, T. N. Wight, K. Sueishi, *Arterioscler. Thromb. Vasc. Biol.* **2007**, *27*, 1159.
[48] K. Sakakura, M. Nakano, F. Otsuka, E. Ladich, F. D. Kolodgie, R. Virmani, *Heart Lung Circ.* **2013**, *22*, 399.
[49] M. R. Bennett, S. Sinha, G. K. Owens, *Circul. Res.* **2016**, *118*, 692.
[50] X. Gu, S. Xie, D. Hong, Y. Ding, *Sci. Rep.* **2019**, *9*, 7461.
[51] B. Dorweiler, M. Torzewski, M. Dahm, V. Ochsenhirt, H. A. Lehr, K. Lackner, C. A. Vahl, *Thromb. Hemost.* **2006**, *95*, 182.
[52] J. Beck-Joseph, S. Lehoux, *Front Cardiovasc. Med.* **2021**, *8*, 737934.
[53] Q. Cai, L. Lanting, R. Natarajan, *Arterioscler., Thromb., Vasc. Biol.* **2004**, *24*, 2263.
[54] D. Nandy, Y. W. Asmann, D. Mukhopadhyay, A. Basu, *J. Cell. Mol. Med.* **2010**, *14*, 1396.
[55] Q. Zhang, S. Wu, G. Sun, R. Zhang, X. Li, Y. Zhang, F. Huang, D. Yuan, *Ann. Transl. Med.* **2021**, *9*, 234.
[56] J. E. Kanter, F. Johansson, R. C. Leboeuf, K. E. Bornfeldt, *Circ. Res.* **2007**, *100*, 769.
[57] G. Booth, T. J. Stalker, A. M. Lefer, R. Scalia, *Diabetes* **2002**, *51*, 1556.
[58] C. A. Cuff, D. Kothapalli, I. Azonobi, S. Chun, Y. Zhang, R. Belkin, C. Yeh, A. Secreto, R. K. Assoian, D. J. Rader, E. Pure, *J. Clin. Invest.* **2001**, *108*, 1031.
[59] D. A. Allen, M. M. Yaqoob, S. M. Harwood, *J. Nutr. Biochem.* **2005**, *16*, 705.
[60] Z. Huang, V. B. Kraus, *Nat. Rev. Rheumatol.* **2016**, *12*, 123.
[61] H. Yuan, C. N. Perry, C. Huang, E. Iwai-Kanai, R. S. Carreira, C. C. Glembotski, R. A. Gottlieb, *Am. J. Physiol. Heart Circ. Physiol.* **2009**, *296*, H470.
[62] P. Waltz, E. H. Carchman, A. C. Young, J. Rao, M. R. Rosengart, D. Kaczorowski, B. S. Zuckerbraun, *Autophagy* **2011**, *7*, 315.
[63] W. C. Dissanayake, J. K. Oh, B. Sorrenson, R. P. Shepherd, *Biosci. Rep.* **2021**, *7*, 41.
[64] M. R. Dasu, S. Devaraj, I. Jialal, *Am. J. Physiol. Endocrinol. Metab.* **2007**, *293*, E337.
[65] Y. Gonzalez, M. T. Herrera, G. Soldevila, L. Garcia-Garcia, G. Fabián, E. M. Pérez-Armendariz, K. Bobadilla, S. Guzmán-Beltrán, E. Sada, M. Torres, *BMC Immunol.* **2012**, *13*, 19.

